Carbonates and Evaporites (2024) 39:33
https://doi.org/10.1007/s13146-024-00944-7

ORIGINAL ARTICLE

Soft-sediment deformation structures or microbially induced sedimentary structures: the description and possible origin of the "loopites" in the Mesoproterozoic Wumishan Formation, North China

Kai Lu[1] · Zhidong Bao[2] · Jin Li[1]

Accepted: 2 February 2024 / Published online: 11 March 2024

Abstract
Within the lower Wumishan Formation at the eastern edge of the Tai-hang Mountains in North China, a ~ 10 m stratigraphic interval contains alternately "bright and dark" laminites with enigmatic loop structures (2.5–27.5 cm in length and 0.6–12 cm in height), preserved in cross-sectional and named "loopites" in this study. The loopites are composed of cores and annulate laminations. Based on the different morphologies, they can be divided into three different types: type I, II and III. Although the loopites are similar to the loop beddings, the formation mechanisms are different. The former is possibly microbially induced sedimentary structures (MISS), while the loop beddings preserve evidence of soft-sediment deformation structures (SSDS) such as boudinage or chain structures, joints and small-scale tensional faults. All three types of loopites have cores. The type I core is made up of relicts of previous microbial mat and the microhighlands, while the type II and III loopites have cores defined by debris and rock fragments. The cores are completely wrapped by microbial mats of later generation. Thus, we can conclude that the formation of loopites is due to the growth, wrapping and deposition of microbial mats, while loop beddings are generated by external triggering mechanism such as earthquake. Furthermore, the discovery and possible formation of loopites may provide a new type of MISS and indicate a stable, anoxic and carbonate-supersaturated environment favorable for microbial mats to form annulate structures, which are controlled by illumination, microtopography and hydrodynamics.

Keywords Mesoproterozoic carbonate · Wumishan Formation · Microbially induced sedimentary structure · Microbial mat

Introduction

The Mesoproterozoic strata, widely deposited in North China, record the detailed geological history of the Earth's evolution in the ancient world from 1.8 to 0.8 Ga (Ying et al. 2011; Tang et al. 2016; Tan et al. 2021). In particular, the widely distributed and well-preserved outcrops of the Mesoproterozoic Wumishan Formation preserve abundant natural information, including paleogeography, paleoclimate, paleontology, paleotectonics, and paleomagnetism, and thus provide excellent research materials for geologists from all over the world. (Zhang 1985; Chen et al. 2013; Li et al. 2013; Mei and Maurice 2013; Tang et al. 2014, 2015; Shen et al. 2018; Yang et al. 2022). The Wumishan Formation is renowned for its large thickness (the thickest outcrop > 3000 m) of dolomitic and various microbial deposits whose main types include various forms (laminated, wavy, cone-shaped, columnar and domal) of stromatolites, thrombolites, and oncolites (Cao 1991; Mei et al. 2008; Tang et al. 2013b; Lu et al. 2019, 2021; Zhai et al. 2023). Moreover, it contains a variety of different types of soft-sediment deformation structures (SSDS) and microbially induced sedimentary structures (MISS) which have attracted the attention of geoscientists in the last three decades.

✉ Kai Lu
kailu_1234@163.com

Zhidong Bao
baozhd@cup.edu.cn

[1] Petroleum Exploration and Production Research Institute, SINOPEC, Beijing 102206, China

[2] College of Geosciences, China University of Petroleum-Beijing, Beijing 102249, China

The earliest record of SSDS in the Wumishan Formation was found in the Xishan section, which is located northwest of Beijing (Song 1988). There are more than 15 types of SSDS (e.g., liquefied mixed layers, diapirs, liquefied veins, liquefied convolute beddings, plate-spine breccia structures, thixotropic diapirs, thixotropic wedges, thixotropic veins, mound-and-sag structures, ball-and-pillow structures, loop beddings, undulated deformations, deformed stromatolites, load casts, flame structures, and chrysanthemum structures) which have been identified in the Wumishan Formation. The major triggering mechanisms in the Wumishan Formation are earthquakes and storms (Xie et al. 1997; Zhang et al. 2007; Qiao and Gao 2007; Qiao and Li 2009; Ettensohn et al. 2011; Su and Sun 2011, 2012; van Loon and Su 2013; Qiao et al. 2017), same as the major perspectives of the triggering mechanisms of SSDS in the world (van Loon 2009; Shanmugam 2017). However, with the development and deepening of research on SSDS, microbial mats and their related structures have usually been observed to be associated with SSDS. Especially in the Proterozoic, microbial mats could be treated as a key factor influencing soft-sediment deformation directly because they were the only biological agents at that time, and their growth could enhance or limit the formation of SSDS (Obermeier 1996; Harazim et al. 2013; Banerjee et al. 2014). Although they were not the major mechanism, they definitely can be a special proxy for representing and recording the SSDS in carbonate and siliciclastic rocks (van Loon and Su 2013; Hill and Corcoran 2018). Thus, in the Mesoproterozoic Wumishan Formation, the microbial mats contributed to the morphologies and perhaps the formation of some SSDS.

The earliest report on loop beddings can be credited to Bradley (1931), which was about lacustrine oil-shale deposits displaying loop beddings from the Eocene Green River Formation, western USA. In addition, a large number of records on the loop beddings had been marked on the different periods and lithologies in the following decades, such as the Devonian and Miocene shales, the Paleogene siltstones and mudstones, and the Ordovician carbonates (Gibling et al. 1985; Trewin 1986; Tian et al. 2006; Yuan et al. 2006). However, the first record of loop beddings in the Wumishan Formation in China was reported by Qiao and Gao (2007); additionally, Qiao and Li (2009) and Su and Sun (2011) documented other loop beddings of the Wumishan Formation in the different outcrops. The origin of the loop beddings is interpreted as the extensional deformations induced by weak earthquakes when the entire laminated soft deposits have not yet been liquefied in a lentic environment (Cavlo et al., 1998; Rodríguez-Pascua et al. 2000). Its cross-sectional view contains closed pseudoconcentric annular layers, and the long axis is parallel to and the short axis is perpendicular to the strata. In addition, the loop beddings usually appear in a chain shape; moreover, the joints present an X-shaped fracture that is caused by tension.

In this paper, we report a problematic annulate structure, which is identified in alternately "bright and dark" laminites of the Wumishan Formation, revealing similar morphological features and forming conditions of the loop bedding, whose laminations are composed of dark layers with high algal matter and bright layers of carbonate particles (Tang et al. 2014). However, it usually appears alone and maintains a good shape of a cross-sectional pseudoconcentric cylinder with no X-shaped fractures on the joints. Meanwhile, its formation is related to microbial activities. For example, for the different mechanisms of SSDS and MISS, one is the "external" force, such as earthquakes, tsunamis and storms, and the other is the "internal" force, which is the cohesiveness from itself. The essential difference between the loop bedding and the problematic annulate structure is the mechanism. Therefore, we named this annulate structure "loopite" and tried to dig into the origin of this structure to determine if it is a special type of loop bedding or a new type of MISS.

Geological setting

Paleoenvironment for the growth of microbial mats in the Wumishan period

Since ~ 1.8 Ga, the breakup of the Columbia supercontinent (Zhao et al. 2003; 2004; 2011) promoted intraplate rifting in the northern part of the Sino-Korean plate to form the Yanliao aulacogen. The development of the epicontinental sea in the Yanliao aulacogen laid the foundation for the deposition of giant thick microbialites in North China. Moreover, the most extensive sea basin of the Yanliao aulacogen was finally formed in the Wumishan period (Lu, 2002; Qiao and Gao 2007); additionally, previous paleomagnetic and paleontological studies of the North China craton showed that it was located near the equator in the Wumishan period (Zhang, 1980; Zhang et al. 1991, 2012), and the paleoclimate was dry and hot (Yan and Liu 1998), with much higher CO_2 and lower O_2 concentrations than today (Kaufman and Xiao 2003). Thus, it provides the most favorable conditions for microbial growth. In addition, the O_2 content in the Proterozoic seawater showed some features of zonation (Canfield 1998), which means that the lower subtidal zone may have been in an anoxic state; the upper subtidal and lower intertidal zones were mainly oxidized with an occasionally anoxic state; and the upper part of the intertidal zone and the supratidal zone were in an oxidized state (Tang et al. 2011; Tang, 2013a). Hence, it can be speculated that the stable and continuous microbial mats were prone to grow in the lower subtidal zone with low energy and anoxic conditions.

The Wumishan Formation

The exposed outcrops of the Mesoproterozoic Wumishan Formation in North China record sedimentary information between ~ 1.52 Ga and ~ 1.47 Ga (Li et al. 2014; Tang et al. 2016), and their thicknesses range from 554.82 m to 3416 m (Zhao et al. 1997; Li et al. 2014) with a decreasing trend from northeast to southwest. The Wumishan Formation is dominated by peritidal carbonates, and the major types of lithologies include massive micritic dolostone, flat, wavy laminated to stromatolitic dolostone, argillaceous dolostone and chert bands and nodules (Fig. 1). The various types of dolostones were deposited under a range of subtidal to supratidal environments (Zhao et al. 1997; Tang et al. 2013a). In general, due to the exposure and the influx of siliciclastic sediments, the microbial mats could develop various forms via growth, destruction and decay. As a result, the MISS were usually found in the intertidal to supratidal zone. However, the loopites are all identified in the relatively thick, intensive and multilayered intervals of laminites that lack MISS. Thus, the loopites were not formed in the same sedimentary environment as the MISS. In addition, stable, continuous and multilaminated biofilms require weeks to months to form (Hill and Corcoran 2018) and must be settled in a stable environment with low energy and low exposure, which supports that loopites are formed in a subtidal environment by the deposition of alternating microbial mats and carbonate particles.

Methods

Fieldwork was conducted in the Wumishan Formation of the Yixian section (N39°8′57″, E115°16′22″), Yixian County, Hebei Province, North China, which is located on the eastern margin of the Tai-hang Mountains, approximately 20 km southwest of Yixian County (Fig. 2A, B). The Wumishan Formation in the Yixian area has unconformable relationships with the underlying Gaoyuzhuang Formation and the overlying Tieling Formation (Fig. 2C). The thickness is approximately 1450 m, and four members (members I–IV) are subdivided in this formation. The lithologies are briefly described in Members I–IV (from bottom to top) as follows: (1) terrigenous clastic rocks on the bottom, dark gray to gray horizontal to wavy-bedded micritic dolostones with cherts; (2) gray to light-gray massive micritic dolostones and algal dolostones with cherts; (3) dark-gray thick-bedded stromatolitic dolostones with thrombolites and cherts; and (4) light-gray thick-bedded dolostones intercalated with cherty bands. Field photos were taken, and rock samples were collected in situ. Thin sections were made of selected specimens for detailed petrographic observation.

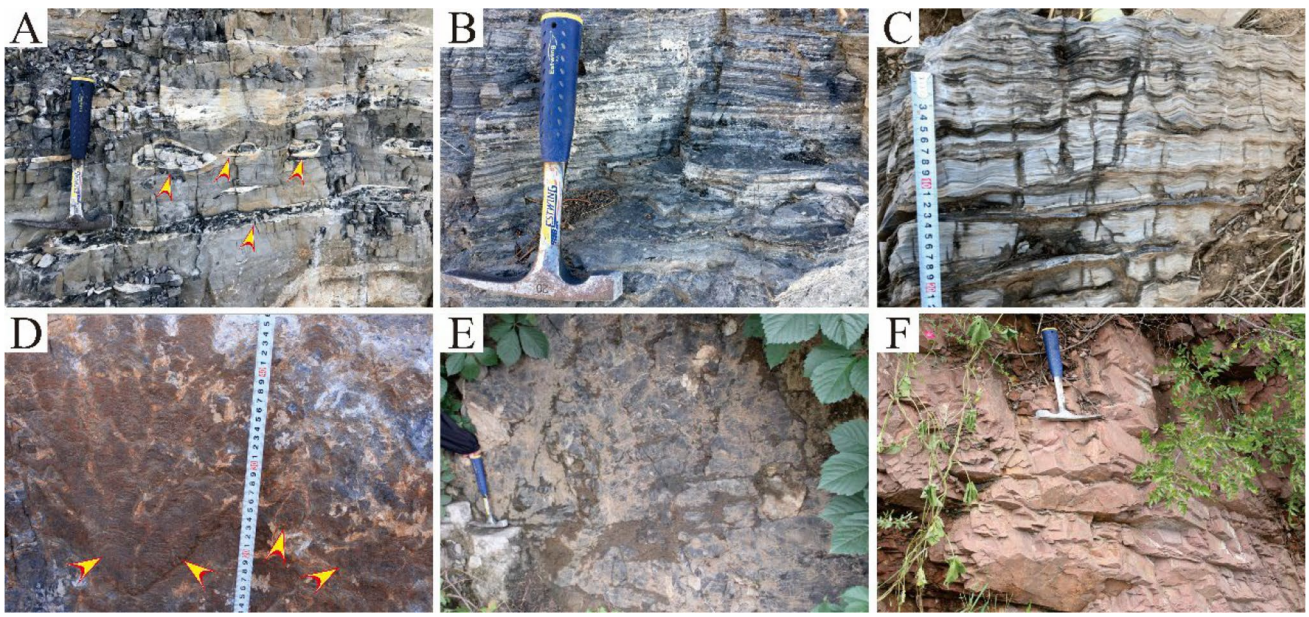

Fig. 1 Some common lithologies of the Wumishan Formation in North China. **A** Massive micritic dolostone with chert (nodules and bands are indicated by arrows), Yixian. **B** Flat laminated dark-gray dolostone, Yesanpo. **C** Wavy laminated gray dolostone, Yixian. **D** Surface-oxidized stromatolitic dolostone; stromatolites are indicated by arrows, Yixian. **E** Dark-gray cherty dolostone, Jixian. **F** Oxidized reddish argillaceous dolostone, Jixian. The three locations are shown in Fig. 2A. The hammer is 28 cm

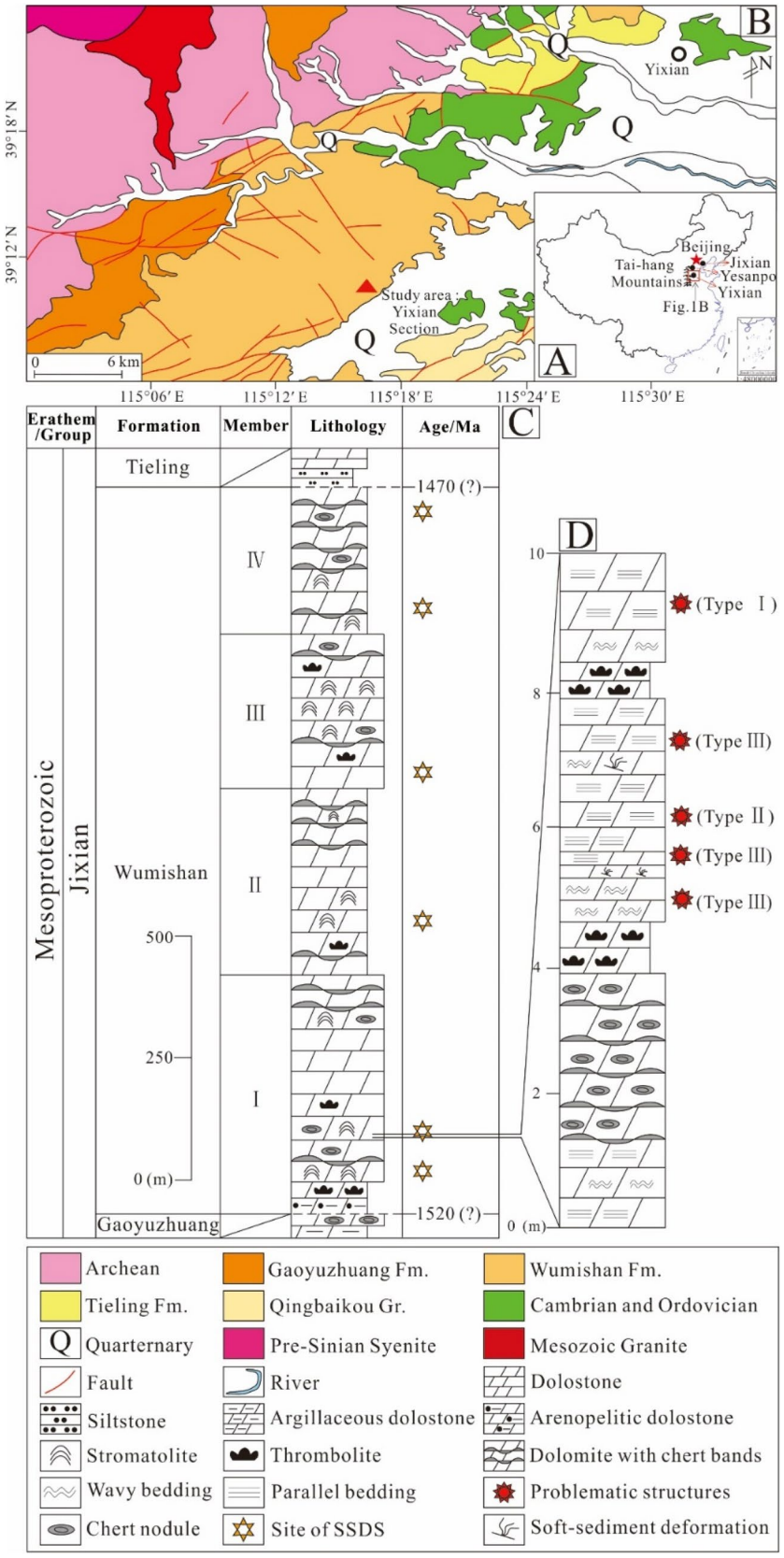

Fig. 2 Regional and local stratigraphy of the Wumishan Formation in the Tai-hang Mountains, China. **A** Locality map with red squares marking the study site in China. **B** Simplified geological map of northeast-central China in the Yixian area, showing the location of the study area. Modified from Zhang et al. 1965. **C** Generalized stratigraphy of the Yixian section. Modified from Tang et al. 2016. **D** Detailed stratigraphic interval in the lower part of Member I of the Wumishan Formation containing the problematic annulate structures

Results

Soft-sediment deformation structures (SSDS)

With the tectonic and sedimentary conditions of intraplate rifting and epicontinental sea, the Wumishan Formation in the Yixian section preserves a wide variety of SSDS. Based on the observations, seven different types of SSDS, including mound-and-sag structures, ball-and-pillow structures, load structures, liquefied veins, plate-spine breccias, convolute beddings, and undulate deformations, have been identified in the Wumishan Formation in the Yixian section, and some apparent features of SSDS are associated with microbial mats.

Mound-and-sag structures

Mound-and-sag morphology in the Wumishan Formation usually develops in dark-gray massive micritic dolostones (Fig. 3A). The typical features of mound-and-sag structures are alternating synclines and anticlines that display different thicknesses of internal layers. The layer is thinner in the mound and thicker in the sag, with undeformed overlying and underlying units.

Ball-and-pillow structures

Ball-and-pillow structures are usually found in the lower part of the Wumishan Formation in the Yixian section. The lithologies of ball-and-pillow structures can be divided into three obvious segments from bottom to top (I, II, III) (Fig. 3B). Segment I is approximately 11 cm in height and comprises light-gray massive micritic dolostones with little lamination and an isolated nodular chert. Segment II (13 cm in height) is dominated by pillow structures and composed of light-gray micritic dolostones with gray curly laminations. In addition, a black cherty subrounded ball structure (8 cm in height, 7 cm in width) was identified in segment II. With the effect of this ball, downlaps of curly laminae occurred at the bottom of the ball. Segment III (> 3 cm in height) contains dark-gray fine-grained cherty dolostones, which are incompletely displayed in Fig. 3B. The grain size becomes increasingly coarser from segments I to III, which means that the overlying segment has a larger density than the underlying segment.

Load structures

Load structure is a liquefaction deformation structure, which is an important type of SSDS. The deformation mainly occurs at the contact interface where lithology changes, and the major deformation mode is that the sediments move upward and downward (Qiao et al. 2017). In general, the load structure is formed by the overlying denser sediments sink into the less dense sediments. But a unique load structure has been recognized in the lower part of the Wumishan Formation in the Yixian section. The uniqueness seems to be that the less dense sediments squeezed into the underlying denser grained sediments. The observed overlying whitish micritic dolostones sank into the light-gray thrombolitic (coarser) dolostones (Fig. 3C).

Liquefied veins

Liquefied veins are one of the most numerous deformation structures in the study area. Vein-type structures are formed in the interbedding of dark and light color layers dolostones (Fig. 3D). The bright laminations are composed of carbonate particles, and the dark laminations are dark-gray algal dolostones that are composed of microbial mats. The sizes of liquefied veins are approximately a few centimeters to 20 cm. Two types of liquefied veins are identified: horizontal veins, which flow along the bright laminations, and vertical veins, which flow vertically towards the laminations.

Plate-spine breccias

The first record of plate-spine breccias in China was from Song (1988) in the Wumishan Formation of Ming Tombs section on the northwest side of Beijing. After that, such breccias are widely identified and observed in the Mesoproterozoic Formations in the North China craton. Plate-spine breccias or accordion folds (Ettensohn et al. 2011), a common type of SSDS, can be found in all members of the Wumishan Formation in the Yixian section. The plate-spine structure is formed in thin laminated dolostone or cherty dolostone layers. Because of the strong compression, the plate-like and band-like soft-sediment layers are squeezed from a horizontal position to an inclined and even vertical position. The lithologies of these breccias could be the same as those of their parent rocks, such as dark-gray chert dolostone and light-gray micritic dolostone (Fig. 3E), and the lengths of breccias range from 0.5 cm to more than 5 cm. In the Yixian section, this type of deformed structure is usually observed between two undeformed layers.

Convolute beddings

Convolute beddings are most common in the interbedded light-gray micritic dolostones and black algal dolostones with thin lamination intervals in the lower part of the Wumishan Formation in the Yixian section. These beds display complex syn-sedimentary folds that are highly deformed and disrupted and show dimensions up to 8 cm in height and

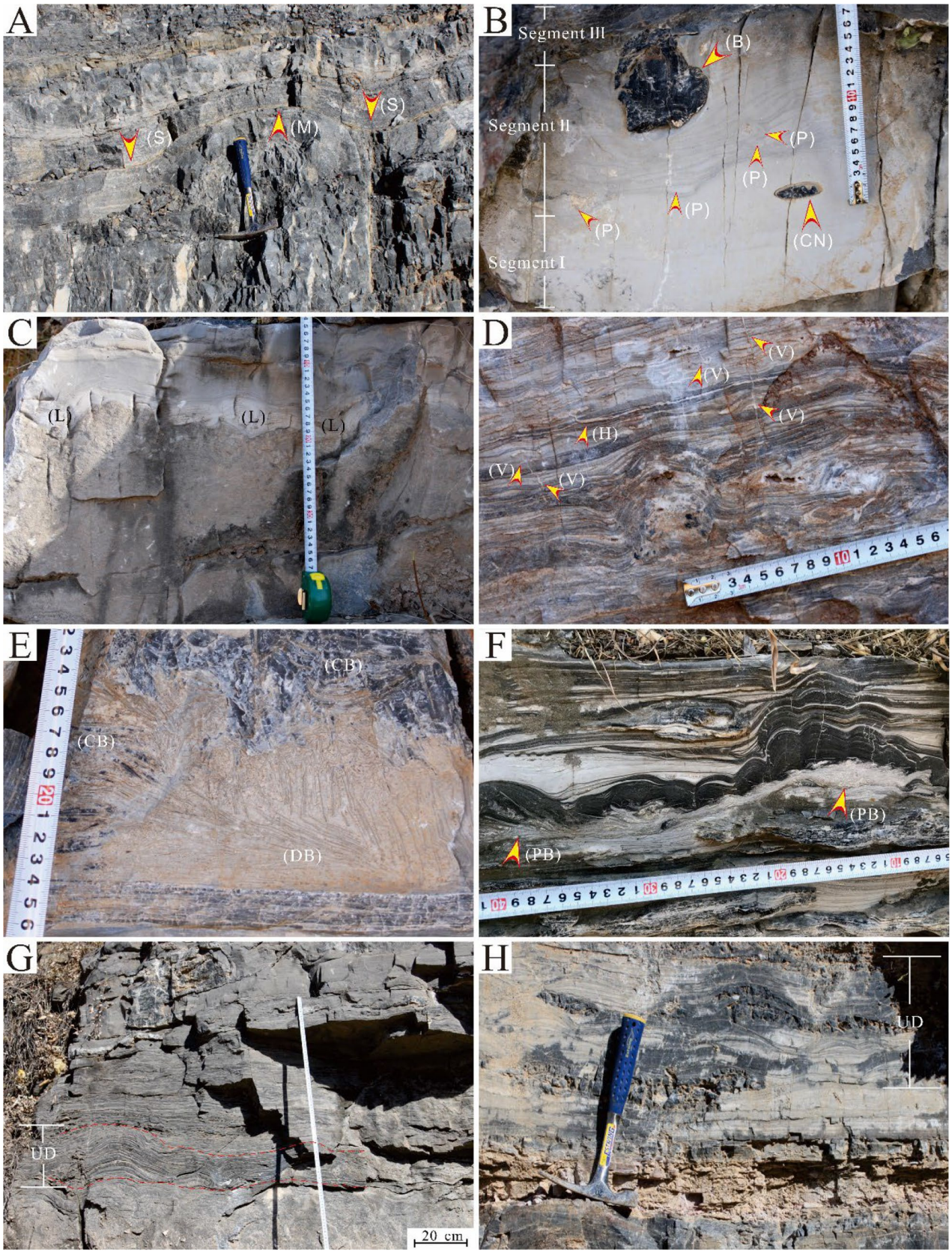
A
(S)
(M)
(S)
B
Segment III
Segment II
Segment I
(B)
(P)
(P)
(P)
(P)
(CN)
C
(L)
(L)
(L)
D
(V)
(V)
(V)
(H)
(V)
(V)
E
(CB)
(CB)
(DB)
F
(PB)
(PB)
G
UD
20 cm
H
UD

◂**Fig. 3** Major types of SSDS identified in the Wumishan Formation of the Yixian section. **A** Mound-and-sag structure from Member III, showing that the thickness of strata increased in the sag (S) and decreased in the mound (M). **B** Ball-and-pillow structure from Member I, showing a chert nodule (CN) in segment I, pillows (P) in segment II and a ball in segment III. **C** The unique load structure (L) from Member I, showing that the layer with low-density sinks into the layer with high density. **D** Liquefied veins from Member II, showing two types of veins: horizontal veins (H) and vertical veins (V). **E** Plate-spine breccias from Member I, and two types of breccias identified: cherty breccia and dolomitic breccia. **F** Black convolute beddings from Member I overlying the plate-spine breccias (PB). The scale tape was placed upside down for convenience of photo taken in the field, and the original photo was not rotated. **G** and **H** Undulate deformations (UD) identified in Members I and III, respectively. The hammer is 28 cm

40 cm in width with the intensity of convolution declining upwards (Fig. 3F).

Undulated deformations

Undulate deformation, an indicator of weak compression, is commonly found between two undeformed layers. This type of SSDS can be identified in various structural backgrounds, depositional environments, and lithologies. Moreover, the scale of undulating deformations was measured over a broad range, from several centimeters to meters. Most undulate deformations, showing dimensions up to 80 cm in height and 2 m in width, are observed in the middle part of the Wumishan Formation in the Yixian section. The undulated layers usually formed in the thin gray laminated dolostones between the undeformed underlying and overlying layers (Fig. 3G and 3H).

Stratigraphic context and depositional environment of loopites

Loopites are identified in the lower part of Member I in the Wumishan Formation in the Yixian section (Fig. 2C). Based on the results of observation, these loopites are preserved on multiple bedding surfaces. Moreover, according to the different morphologies, the loopites can be divided into three types: types I, II and III.

The stratigraphic interval preserving type I is the laminites with bright laminations, which are massive to laminated micritic dolostones, and dark laminations, which are algal dolostones (Fig. 4A). From bottom to top, the morphologies of the laminations change from wavy to horizontal, and the stable and thickly developed laminites show that the hydrodynamic force gradually weakens, which demonstrates the depositional features of the lower subtidal zone. Type I loopite develops between two horizontal layers of laminites and is ~ 5 cm thick (Fig. 4B).

Type II is preserved in a 10 cm thick gray dolostone interval with very thin and intensive laminations (Fig. 4C). The thickness of each lamina is thinner than type I, and the overall hydrodynamic force is weaker, indicating the sedimentary environment of the lower part in the lower subtidal zone.

The stratigraphic interval of type III is composed of gray to light-gray wavy-bedded micritic dolostones, which are above the grayish massive grain dolostone (Fig. 4D, E). The major types of grains are round punctate thrombolites and tabular thrombolites with blocky mesoclots (Fig. 4F). Moreover, the distribution of round punctate thrombolites was disturbed downwards, stratified and distributed upwards. In addition, the same characteristics of wavy-bedded deposition were observed on other two outcrops separated by a few meters, and intense SSDS intervals were identified under the wavy beds (Fig. 4G, J). Comprehensively analyzing, the wavy feature means a stronger hydrodynamic force; hence, type III is deposited in the upper part of the lower subtidal zone, and the intervals containing type III show a weaker hydrodynamic force from bottom to top.

Morphological description of loopites

The loopites are present along the long axis in the cross-sectional view, so the annular laminations can be clearly exhibited. Type I (3.5–12.5 cm in length and 0.6–2 cm in height) developed in the laminites and appear alone or in discontinuous chain shape (Fig. 4A, B). The core of type I is black strip-shaped algal micritic dolostone, and the annulate laminations are composed of thick layers of continuous dark-gray algal dolostones with discontinuous white micritic dolostones, which show the blurry morphology of a cross-sectional pseudoconcentric cylinder.

Type II (2.5–5 cm long and 1–2 cm wide) usually appears alone with a poor sectional cylindrical shape; meanwhile, the top-covered laminations exhibit the obvious features of pinching and shrinking on the ends of loopites (Fig. 4C). In general, the core is relatively small, and the laminations above the core are more curved than those below.

Type III (11.5–27.5 cm long and 5–12 cm wide) appear alone or stacked with each other and are not preserved in the chain shape. The annulated laminations of type III clearly display features of interbedding of dark and light color layers and good curvature on the ends. The core is a long strip of dark-gray algal micritic dolostones 3.5–25 cm in length and 2–5 mm in height (Fig. 4E, I, J). Since the largest dimension of type III is incomplete in the section, only half of the part is visible. Thus, the actual length of the whole loopite should be longer.

According to the stratigraphic context, the loopites deposited in a relatively weak hydrodynamic environment lacking the impacts of tectonics. However, considering the stratigraphic interval and morphology, the sedimentary

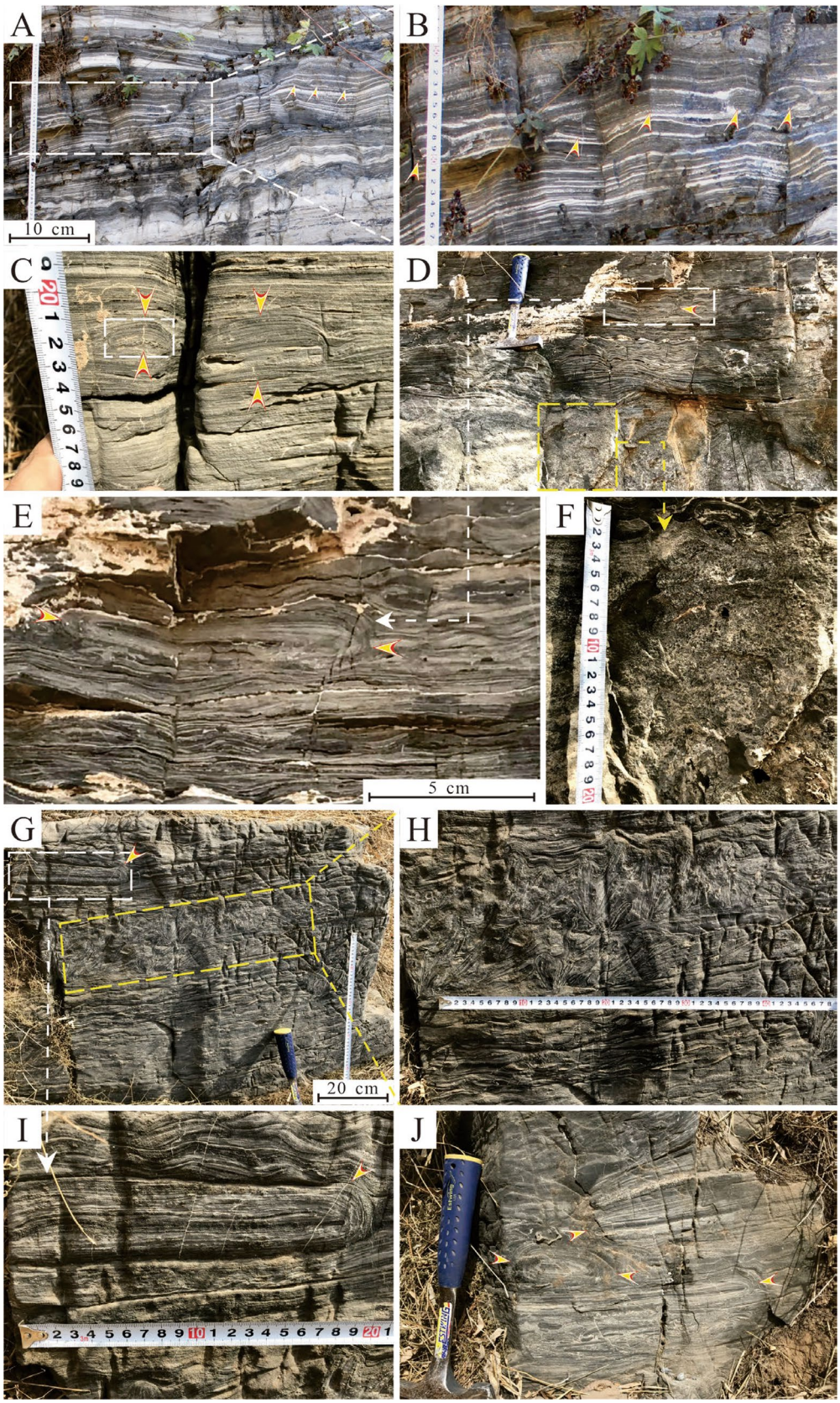
A
10 cm
B
C
D
E
5 cm
F
G
20 cm
H
I
J

◂**Fig. 4** Photographs of problematic loopites in the Wumishan Formation in the Yixian Section. All loopites are highlighted by arrows. **A** and **B** Type I are preserved in the dark-gray laminites. The white dashed square shows the area of **B**. **C** Type II laminae are identified in the intensive laminites with curved shapes, and the white dashed square shows the sampling site in Fig. 5C. **D** and **E** Type III are in the wavy-bedded intervals. The hammer is 28 cm. The white dashed square shows the area of **E**. **F** The yellow dashed square in **D** shows the grayish massive grain dolostone with thrombolites. **G** Type III are in the wavy-bedded intervals. The white dashed square shows the area of **I**. **H** The yellow dashed square in **G** shows the plate-spine breccias preserved below type III. **I** and **J** Type III are preserved in the wavy-bedded intervals. The hammer is 28 cm

environment of each loopite type is virtually different. Type III deposited in the relatively strongest hydrodynamic environment with the largest size among the three types. Type II is the smallest type with the weakest hydrodynamic force, and type I is the moderate type. Thus, the different hydrodynamic environment determined the different types of loopites.

Discussion

Triggering mechanism of SSDS

According to the results of comprehensive observations, the major triggering mechanism of SSDS in the Wumishan Formation is earthquake. The mound-and-sag structures occurred during the episode of deposition with unconsolidated sediments and was triggered by earthquake-induced transtensional and compressional shear stress (Rossetti and Goes 2000; He et al. 2021). When an earthquake occurs, the vibration could make the overlying liquefied sediments separate from the parent rock and form balls or pillows floating in the underlying less dense sediments (Ezquerro et al. 2015). The unique load structure is a driving force system related to gravitational instability (Zhong, et al. 2017). But because of the differences in densities, it was impossible to form load structures under geostatic pressure. Only in the strong earthquake-triggered situation did the underlying layers have stronger liquefaction than the overlying layers, which could make the lower density layers sink down to form that load structures (Qiao, et al. 2012).

The parent rocks of liquefied veins are micritic dolostone layers that contain pore water, and dissolved air escapes in the lower pressure direction under vibration triggered by earthquakes (He and Qiao 2015). In the study area, the appearance of plate-spine breccias often accompanies convolute beddings because both were formed by compression whose triggering mechanism was interpreted as intense seismic activity (Bhattacharya and Bandyopadhyay 1998; Rossetti 1999; Qiao and Gao 2007; Li et al. 2008; El Taki and Pratt 2012). Moreover, the undulation degree of undulate deformation also depends on the strength of compression caused by earthquakes (van Loon and Su 2013).

The relationship between SSDS and microbial mats

Based on the results of observations, earthquake-induced mound-and-sag structures usually have a relatively large scale, and their features are not necessarily associated with microbial mats. However, it is obvious that the pillow structures can be presented by the deformation of microbial mats (Fig. 3B). Furthermore, the curvature and curl of the soft microbial mats can also increase and lead to soft-sediment deformation. In general, microbial mats are not necessary for the formation of load structures because as long as a density difference exists, gravity or earthquakes can induce deformation. However, if microbial mat intervals appear, they may produce different densities much easier than non-biofilm intervals. Thus, the existence of microbial mats indicates positive effects on the formation of load structures. Similarly, it seems that the formation of vein-type structures is not related to the microbial mats because the veins are rooted in the carbonate particle layers (Fig. 3D). However, because of the trapping and binding from the growth of microbial mats, carbonate particles can be cohered and deposited to form heterogeneous laminations (Samanta et al. 2011). Therefore, although the microbial mats are not the direct triggering mechanism of forming liquefied veins, they contribute to producing the material basis of the liquefied veins.

Apparently, compared with the above types of SSDS, the relationship between plate-spine breccias and microbial mats becomes tighter, and it can be interpreted that the initial forms of the breccias are laminites with horizontal laminations, which are consolidated or unconsolidated microbial mats (Su and Sun 2012). This is why plate-spine breccias cannot be found in massive or homogeneous rocks. As a result, microbial mat-related laminites can be an indispensable precondition for plate-spine breccias. The most common SSDS in the Wumishan Formation are various convolute beddings and undulate deformations, which are formed by the deformations of initially horizontal laminations that are formed from alternating deposited microbial mats and carbonate particles. Hence, even if the blackish beddings and the gray laminations had been convoluted or undulated (Fig. 3F, G, H), it is obvious that the original form of these convolute beddings was flat multilayered microbial mats. This phenomenon is ascribed to the fact that microbial mats are the only biological agents that form laminar deposits in Mesoproterozoic carbonates. Consequently, earthquakes are the triggering mechanism, but the existence of microbial mats is a prerequisite for the two types of SSDS. The microbial mats are not only the material basis for forming the convolute beddings and undulate deformations but also the convolute and undulate microbial mats are precisely the

SSDS themselves. Evidently, the major functions of microbial mats for SSDS are producing the material basis or the proxy to exhibit SSDS, not as the major triggering mechanism. Indeed, because of the close relationship between SSDS and microbial mats in the Wumishan Formation, it is easy to confuse our first found loopites with loop beddings.

Possible origin of the loopites

Therefore, we interpret the unusual loopites as the previously undescribed MISS, mainly based on the following observations and analyses: (1) The laminations of loopites display distinct interbedding of dark and light color layers, which is the typical feature formed by the growth of microbial mats. (2) Every loopite contains a core, and the types of the cores can be rock debris (Fig. 5C) or strip-shaped algal dolostones (Fig. 5A). In addition, the number of top-covered layers of the core is greater than the number of underlying layers, which demonstrates the growth of microbial mats (Fig. 5C). (3) Even though the cores of the loopites are not circular, the wrapping laminations on the edges demonstrate good roundness and curvature, which is an obvious feature of sedimentary structure. The loop beddings or boudinages formed by the compressive or tensile stress generated by tectonic movement do not have this feature. (4) The laminations are growing around the core layer after layer. The most direct evidence is that the formation stage of the loopites is observed on the type I outcrop. In Fig. 5B, a single strip-shaped black-gray algal dolostone (35 cm in length and 1.5 cm in height) becomes the core of a type I in the interval of laminites. Then, the outer layer with the same lithology wraps the core from top to bottom. The left and right ends exhibit a good but incomplete arc shape, and the left curves better than the right. The bottom surface of the core presents the features of light-gray microbial dolostones, indicating that the microbes were aggregating along the bottom to form new microbial mats. Furthermore, due to the influence of the loopite, the upper laminations are bent to cover the loopite, and the degree of curvature on the left side is higher than that on the right, which has the same trend as the curvature

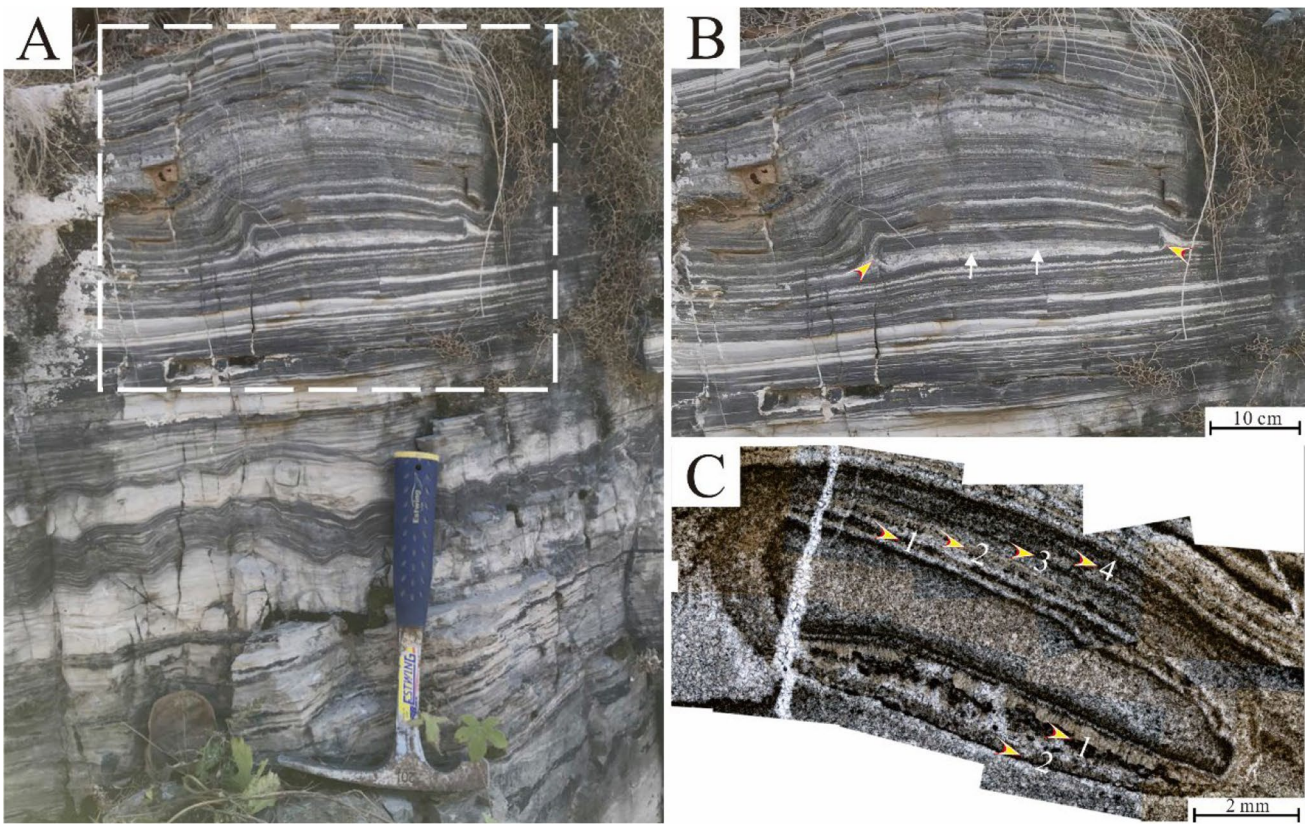

Fig. 5 Photographs showing clues of microbial sedimentary origin. **A** The formation stage of loopites is observed on the type I outcrop. The hammer is 28 cm. **B** The white dashed square in **A**. The outer layer curved and wrapped the core from top to bottom (yellow arrows), and the white arrows indicate that the microbes aggregated under the core. **C** Photograph of type II, which is stitched by 11 photomicrographs of different parts, indicating the morphology of the core and algal layers of type II. The total thickness of the four overlying laminations is larger than that of the two underlying laminations, but each single overlying laminations is thinner than the underlying laminations

of the two ends of the loopites. In addition, the lower laminations below the loopite maintain a horizontal shape without deformation. This further illustrates that loopite is the structure caused by microbial activity during deposition, and the growth rate of microbial mats above the core is larger than that below the core.

Compared with other special structures, such as lenticular-flaser structures, pseudonodules, and various types of microbialites in the Proterozoic strata (Song and Gao 1985; Bhattacharya and Bandyopadhyay 1998; Guo, et al. 2013; Rasmussen, et al. 2009), it is difficult to classify the loopites into one certain type due to their unique morphologies. In addition, concentric laminae are usually deemed to have formed by related microbial activities in a high hydrodynamic environment (Pufahl et al. 2013; Diaz et al. 2017). However, we strongly agree that the possible origin of the loopites is related to the growth of microbial mats with relatively weak hydrodynamic forces.

In Fig. 6, in the early formation stage of the loopite, a microhighland appeared on the previously formed flat and broad microbial mats. The origin of the microhighland is due to some debris, such as rock debris and fragments of microbial mats, being brought and dropped on the flat microbial mats by the tidal current from the upper part of the tidal flat (Fig. 6-Stage B). Alternatively, the carbonate sedimentation rate increased, which caused the carbonate to be deposited slightly thicker here and changed the original microtopography (Fig. 6-Stage B_1). Through this study, we found that the two possible origins of the microhighland have different effects on the formation and morphologies of the loopites. Therefore, we will discuss them separately.

First, when the microhighland was formed by a dropped rock debris, the microbial mats under the debris sank slightly. Because of this highland, the photosynthesis intensity and deposition rate here are both greater than those in other flat areas. Hence, cyanobacteria are more prone to aggregate together at this spot to form a new microbial mat and then cover the top of the rock debris. This process repeats until the thickness of the top-covered microbial mats reaches a certain scale, which causes the rock debris to sink downwards due to gravity. Because of the above pressure, the microbial mats under the rock debris start to sag and bend (Fig. 6-Stage C). Furthermore, the separately top-covered and underlying microbial mats begin to connect and polymerize to each other due to adhesion and adsorption (Fig. 6-Stage D) and then wrap the rock debris to form the loopite (Fig. 6-Stage E). Notably, the loopites with debris cores are distinguished by the thickness of single underlaid annulated laminations being greater than that of top-covered laminations because the formation of underlaid laminations mainly depends on adsorption due to pressure; conversely, the total thickness of the top-covered laminations formed by normal sedimentation of microbial mats is larger than that of the underlaid laminations. Consequently, the stratification of the underlying annulated laminations is weaker and more obscure than that of the top-covered laminations. In our case, types II and III both had the same origin as described above.

Second, if the microhighland was formed by the increased carbonate sedimentation rate, the thickness of the carbonate sediments here will be slightly larger than other flat parts. Similarly, the photosynthesis intensity and deposition rate are higher in this high spot; therefore, cyanobacteria will gather here first to form a new microbial mat that has the same size as the highland (Fig. 6-Stage C_1). As the process was repeated, an increasing number of new microbial mats covered the highland with increasingly larger sizes. Furthermore, the larger microbial mats that cover the initially formed microbial mat began to bend downwards because of currents and gravity, and then the initially formed microbial mat became the core and was wrapped by the top-covered mats (Fig. 6-Stage D_1). However, the poorly stratified carbonate sediments below the core are too thick to bend; therefore, the underlying microbial mats are difficult to polymerize with the top-covered mats via adhesion or adsorption. Simply, the annulated laminations of this type of loopite are mainly formed by the top-covered microbial mats wrapping downwards and assisted by the adsorbed microbes on the bottom of the core (Fig. 6-Stage E_1). Obviously, type I in our study relies on the formation described above with obscure laminations and smaller thicknesses.

Possible environmental controls on the loopites

The Wumishan Formation was deposited in the half-graben basin of the Yanliao aulacogen (Chen 1983; He et al. 2000), which was formed by the extensional rifting of the North China Block during 1.8–1.6 Ga (Cao 2002; Peng et al. 2004) because of the breakup of the Columbia supercontinent (Zhao et al. 2003; 2004; 2011). A series of NE- and NW-striking syngenetic faults developed in the Yanliao aulacogen (Qiao and Gao 2007), which were generated by intraplate rifting and induced strong earthquakes. The ample records of earthquake-induced SSDS in the Wumishan Formation in the Yixian section, which is located near the major NE syngenetic Lingyuan–Miyun fault (Zhang et al. 2007), verify that the development and distribution of SSDS in the Wumishan Formation were controlled by the axial faults in the Yanliao aulacogen. Based on our detailed analyses of the outcrops, SSDS can be identified in all members of the Wumishan Formation in the Yixian section; however, the overall tendency shows that the types and frequencies of SSDS decrease from Members I–IV, which may reveal that during the depositional period of the Wumishan Formation, the effect of paleoearthquakes became weaker, and the Yanliao aulacogen entered a relatively stable stage from a strongly extensional stage.

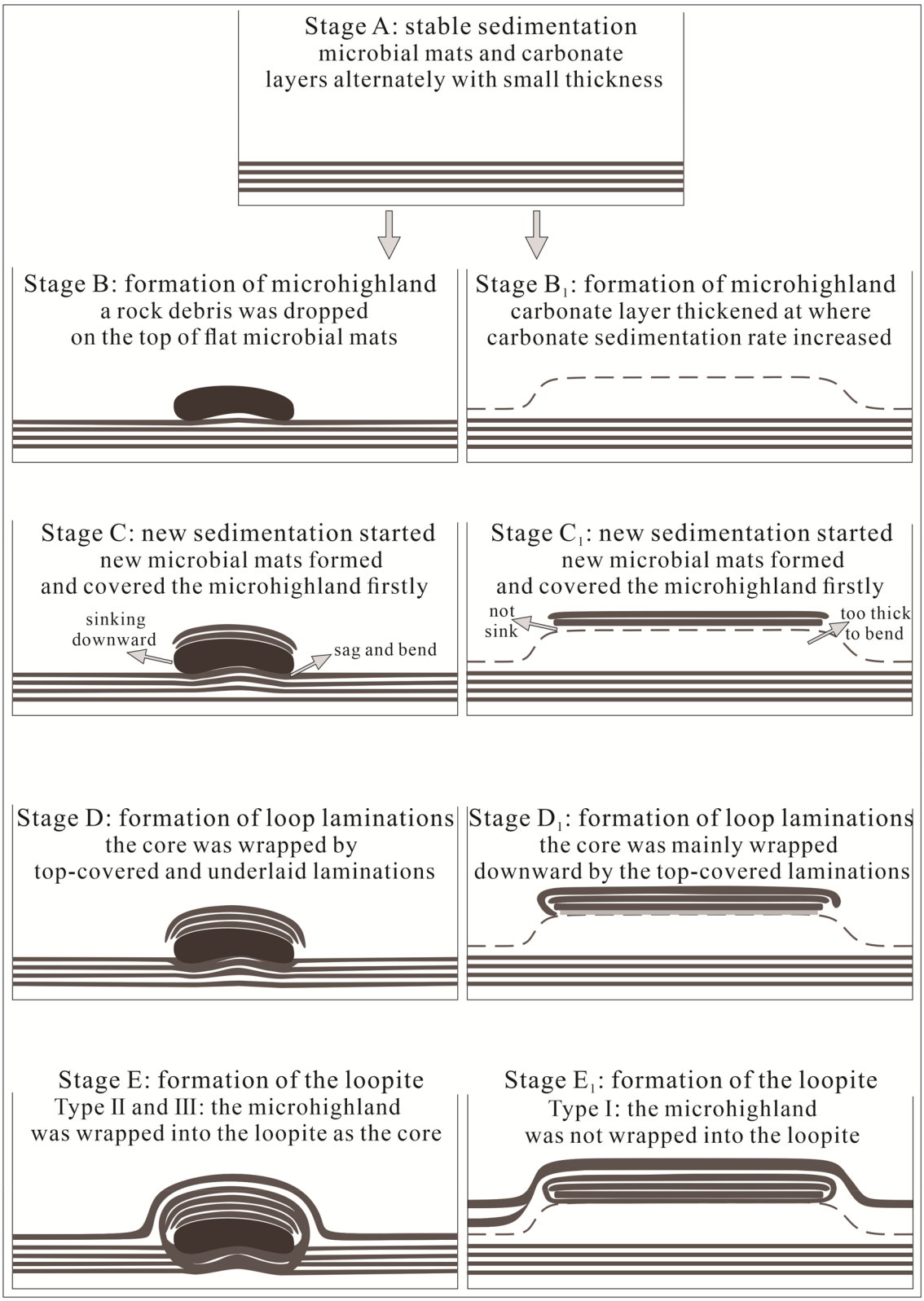

Fig. 6 Two possible forming processes of the different types of loopites. Stage **A**–**E** shows the forming process of types II and III. Stage **A**–**E**$_1$ shows the forming process of type I

The deposition of the Gaoyuzhuang Formation (1.6 Ga?–1.54 Ga?) (Tang et al. 2022) is the response of the first massive transgression of the Jixianian, representing the main deposits of the Yanliao aulacogen entering the sedimentary stage of the epicontinental sea (Huang et al. 2001) until ~ 1.4 Ga (Pan et al. 2013), which further demonstrates that the North China Block entered the relatively stable stage from the cracking of the Columbia supercontinent (Zhang 2004). Consequently, under such a depositional background, a transgression occurred in the early deposition of the Wumishan Formation to deposit thick intervals of laminites, and loopites are identified in such laminites that contain densely packed interbedding of dark and light color laminations (Fig. 4A–D), which are composed of abundant microbial remains in the dark laminations, suggesting a biogenic origin (Fig. 5A–C). The dark laminites in the Wumishan Formation in the Yesanpo section are considered the products of subtidal lagoons and contain no current- or wave-influenced sedimentary structures (Tang et al. 2014). However, this kind of laminite dominates Member I of the Wumishan Formation in the Yixian section, implying a different sedimentary environment.

In terms of dominance, the laminites occur in the lower subtidal facies, and from the lower to upper part of the lower subtidal zone, their laminations change from horizontal to wavy forms (Fig. 4A–D), which provides evidence that hydrodynamics are an important control on the development of laminites. In the same way, with the change in hydrodynamics, the morphologies and sizes of loopites are altered. Due to the initial transgression of the Wumishan Formation, the types of sediments change from ooids (Fig. 7A–C) to tabular thrombolites (blocky to round punctate mesoclots) (Fig. 7D) to laminites (wavy to horizontal). This clear tendency suggests that the depositional environment changes from a lower intertidal to a lower subtidal zone with continuously weakened hydrodynamic forces, which are controlled by rising sea level in a broad environment.

Apparently, three different types of loopites occur in three different types of laminites (Fig. 4A, C, D), and the common prerequisite for forming the loopites is abundant microbial mats (Fig. 7E), which are derived from the increase in Mesoproterozoic microbial abundance (Riding 2006). However, calcified cyanobacteria were barely found in the laminations of loopites, which possibly demonstrates that p (CO_2) is much larger than 10 PAL (present atmosphere

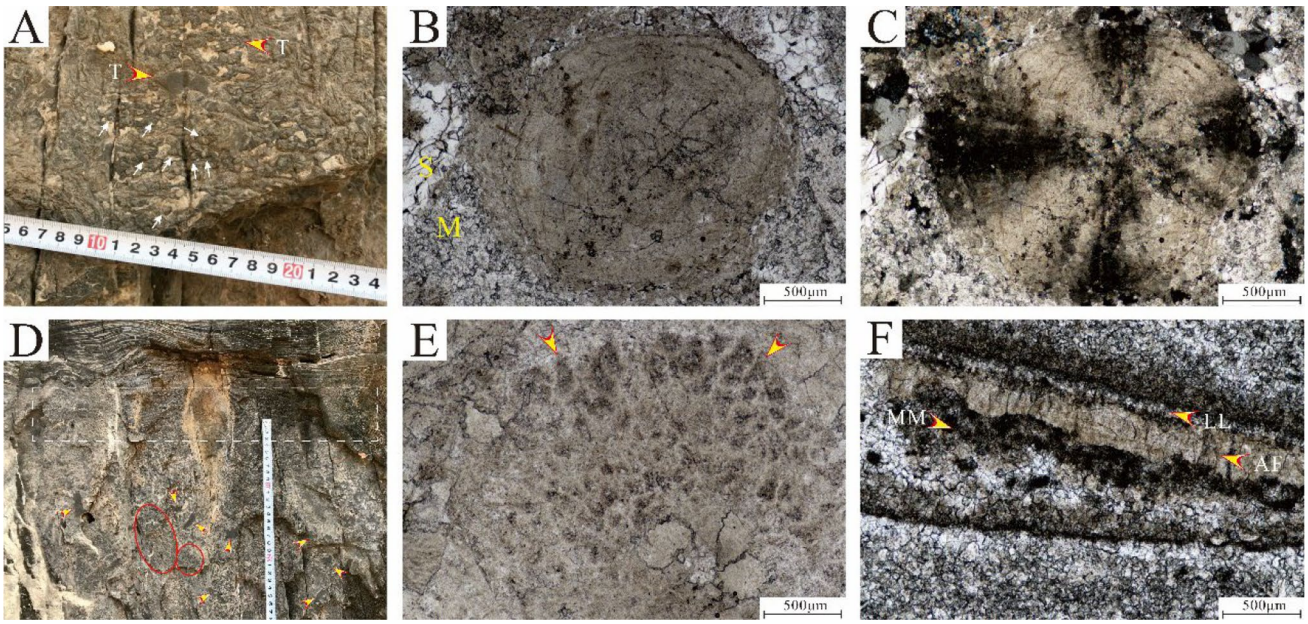

Fig. 7 Macro- and microscopic features of different types of sediments from the lower intertidal to lower subtidal areas of the Wumishan Formation. **A** Photo of an outcrop showing the lower intertidal facies; because of the strong hydrodynamics, ooids (white arrows), which are the main sediments, are mixed with thrombolites (T). **B** Plane-polarized and **C** cross-polarized light photomicrographs showing textures of a radial ooid, which is surrounded by micritic matrix (M) and spar-filled voids (S). **D** Photo of outcrop showing the upper subtidal facies; the main sediment type is thrombolites. The clear tendency of the large blocky mesoclots of thrombolites (yellow arrows) changes to small round punctate clots (white dashed square) from bottom to top, which suggests that the hydrodynamics become weaker. Microbial-related structures (red circles) are identified to reveal high microbial biomass. **E** Photomicrographs showing the microbe colony (yellow arrows) in the micritic dolostone, which presents arbuscular and fan-shaped forms. The sample is collected from **D**. **F** Plane-polarized photomicrographs showing the textures of laminations of loopites in the lower subtidal facies, which contain clear alternations of dark microbial mats (MM), fibrous aragonite (AF) and light micritic laminations (LL)

level) (Riding 2011). In addition, the precipitation of fibrous aragonite was identified in the laminations of laminites and loopites (Fig. 7F), which may indicate that the carbonate saturation was much higher than that in modern oceans and that the bacterial sulfate reduction (BSR) played an important role in consuming organic matter and sulfate to produce bicarbonate to ensure precipitation, which means that loopites were deposited in an anoxic and carbonate-supersaturated environment with a relatively high microbial biomass (Grotzinger and Kasting 1993; Grotzinger and Knoll 1999; Brocks et al. 2005; Tang et al., 2013c). Thus, under possible similar environmental conditions, the advent of loopites is controlled by the activities of the microbial community, which can be influenced by illumination and microtopography, and their morphologies and sizes are controlled by hydrodynamics. Due to phototropism, microbes preferentially grow on the microhighlands to obtain stronger illumination to increase the growth rate, which would produce thicker laminations (Diehl 2002; Tang et al. 2014), reflecting that the environment influences the activities of the microbial community and the sensitivity of the microbial community to changes in the environment. Moreover, when the hydrodynamics become stronger, forming the annular stromatolitic structures of loopites is the response and reactivity of microbes against and slows down the water flow to maintain the proper weak hydrodynamic environment for their growth. Thus, as the hydrodynamics become increasingly stronger, the sizes become increasingly larger (Fig. 8). As a result, type II develops in the deepest and weakest hydrodynamic environment and contains the thinnest laminations and smallest size. Conversely, type III forms the largest size because of the shallowest water depth and strongest hydrodynamics (Fig. 8). In addition, this is why only the laminations of the loopites retain the horizontal shape along the long axis in the wavy laminites (Fig. 4D and 4G). Thus, the loopites may indicate a relatively weak but frequently changing hydrodynamic environment with relatively high microbial biomass.

Conclusion

Seven different types of earthquake-induced SSDS, which contain obvious tendencies suggesting that the types and frequencies decrease from Members I–IV, have been identified in a well-preserved outcrop of the Wumishan Formation in the Yixian area, which is located near the major NE syngenetic Mesoproterozoic Lingyuan–Miyun fault. The location and the tendency may indicate that the development and distribution of SSDS were controlled by the axial faults in the Yanliao aulacogen; however, the effect of paleoearthquakes became weaker, and the Yanliao aulacogen entered a relatively stable stage from a strongly extensional stage during the depositional period of the Wumishan Formation.

Most SSDS have been identified to be associated with microbial mats. The relationship between SSDS and microbial mats can be interpreted as the microbial mats can provide a material basis and be a proxy for SSDS, but their main function is to form the MISS and to deposit microbialites during their growth. Thus, the biogenic-origin laminites

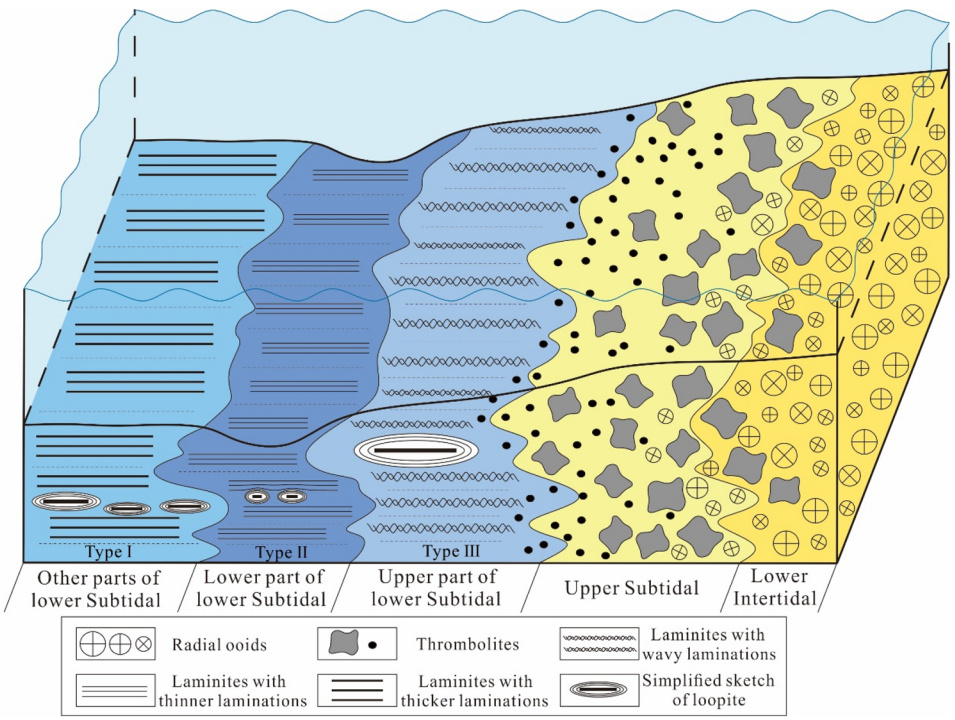

Fig. 8 A sedimentary model suggested for the loopites in the lower subtidal zone, whose sizes are controlled by hydrodynamics, and the change in types of sediments from lower subtidal to lower intertidal facies. Modified from Tang et al., 2013c; 2014

with interbedding of dark and light color laminations were deposited in the lower subtidal facies and dominated Member I of the Wumishan Formation. Moreover, three different types of loopites are identified in three different types of laminites; meanwhile, abundant microbial mats, a lack of calcified cyanobacteria and the precipitation of fibrous aragonite are found in the laminites, demonstrating that the problematic loopites are formed in an anoxic and carbonate-supersaturated paleoenvironment with a relatively high microbial biomass.

Because of the essential difference in the formation, the first found problematic loopites (2.5–27.5 cm in length and 0.6–12 cm in height) from the Mesoproterozoic Wumishan Formation are not loop beddings but belong to examples of a previously undescribed MISS that formed by the growth and wrapping of microbial mats. Based on our reconstructive formation processes and sedimentary model, the formation of loopites is controlled by illumination, microtopography and hydrodynamics. To produce thicker laminations, the microbes will grow on the higher microtopography preferentially to obtain stronger illumination. Meanwhile, to maintain the proper weak hydrodynamic environment for their growth, the microbial mats will grow on the higher microtopography to form the annular stromatolitic structures of loopites to protect against and slow down the stronger hydrodynamics. In addition, as the hydrodynamics become increasingly stronger, the sizes of loopites become increasingly larger. Thus, the significance of the discovery of loopites is not only to provide a new type of MISS, but also to reflect how the depositional environment influences the activities of the microbial community and the sensitivity of the microbial community to changes in the environment. The presence of loopites may suggest a new and pure sedimentary growth mechanism of the microbial mats to form annulate structures in a relatively weak but frequently changing hydrodynamic environment in the Mesoproterozoic period.

The annulate and laminated structures attracted the attention of the global academic community. The proposed genetic model of the loopite in this study provides another new possibility for the formation of annulate and laminated structures. Although the loopite is currently first reported in North China, it is widely distributed in the Mesoproterozoic in North China. Therefore, we believe that scholars around the world will gradually pay attention to this structure and report on it. We look forward to the comparability of loopites in different sites of the world, which can make them a signature structure in the Mesoproterozoic sedimentary environment.

Acknowledgements The authors wish to thank the editor LaMoreaux and two anonymous reviewers for their valuable and helpful comments and suggestions. The authors also thank Pu Wan, Yingzhuo Cao, Ke Zhang and Ruiyu Wang for assistance in the field. This work was co-supported by the Class A Strategic Priority Research Program of the Chinese Academy of Science (No. XDA14010201) and the National Key Research and Development Programs of China (Grant No. 2018YFC0604304).

Author contributions Kai Lu wrote the main manuscript text. Zhidong Bao and Jin Li supervised and revised the manuscript. All authors reviewed the maunscript.

Data availability All relevant data are within the paper.

Declarations

Conflict of interest The authors have no conflicts of interest to declare that are relevant to the content of this article.

References

Banerjee S, Sarkar S, Eriksson GP (2014) Paleoenvironmental and biostratigraphic implications of microbial mat-related structures: examples from the modern Gulf of Cambay and the Precambrian Vindhyan Basin, India. J Palaeogeogr 3:127–144

Bhattacharya HN, Bandyopadhyay S (1998) Seismites in a Proterozoic tidal succession, Singhbhum, Bihar, India. Sediment Geol 119:239–252

Bradley WH (1931) Origin and microfossils of the oil shale of the Green River Formation of Colorado and Utah. U.S. Geological Surv Prof Pap 168:1–58. https://doi.org/10.3133/pp168

Brocks JJ, Love GD, Summons RE, Knoll AH (2005) Biomarker evidence for green and purple sulphur bacteria in a stratified Paleoproterozoic sea. Nature 437:866–870

Calvo JP, Rodríguez-Pascua MA, Martin-Velazquez S, Jimenez S, De Vicente G (1998) Microdeformation of lacustrine laminite sequences from Late Miocene formations of SE Spain: an interpretation of loop bedding. Sedimentology 45:279–292. https://doi.org/10.1046/j.1365-3091.1998.00145.x

Canfield DE (1998) A new model for Proterozoic ocean chemistry. Nature 396:450–453. https://doi.org/10.1038/24839

Cao R (1991) Origin and order of cyclic growth patterns in matministromatolite bioherms from the Proterozoic Wumishan formation, North China. Precambrian Res 52:167–178. https://doi.org/10.1016/0301-9268(91)90018-6

Cao X (2002) The characteristics and origin of iron REE poly-metal deposits related to rift system of middle Proterozoic in the western part of northern margin of North China block. Progr in Precambrian Res 25:246–255 (**in Chinese with English abstract**)

Chen J (1983) A preliminary study on the geological evolution of Sino-Korea paraplatform during middle to terminal Proterozoic. Geol Rev 29:1–8 (**in Chinese with English abstract**)

Chen L, Huang B, Yi Z, Zhao J, Yan Y (2013) Paleomagnetism of ca. 1.35Ga sills in northern North China Craton and implications for paleogeographic reconstruction of the Mesoproterozoic supercontinent. Precambrian Res 228:36–47. https://doi.org/10.1016/j.precamres.2013.01.011

Diaz MR, Eberli GP, Blackwelder P, Phillips B, Swart PK (2017) Microbially mediated organomineralization in the formation of ooids. Geology 45:771–774. https://doi.org/10.1130/G39159.1

Diehl S (2002) Phytoplankton, light, and nutrients in a gradient of mixing depths: theory. Ecology 83:386–398

El Taki H, Pratt BR (2012) Syndepositional tectonic activity in an epicontinental basin revealed by deformation of subaqueous carbonate laminites and evaporites: seismites in Red River strata (Upper Ordovician) of southern Saskatchewan, Canada. Bull Can Petrol Geol 60:37–58

Ettensohn FR, Zhang C, Gao L, Lierman RT (2011) Soft-sediment deformation in epicontinental carbonates as evidence of paleoseismicity with evidence for a possible new seismogenic indicator: Accordion folds. Sediment Geol 235:222–233. https://doi.org/10.1016/j.sedgeo.2010.09.022

Ezquerro L, Moretti M, Liesa CL, Luzón A, Simón JL (2015) Seismites from a well core of palustrine deposits as a tool for reconstructing the paleoseismic history of a fault. Tectonophysics 655:191–205. https://doi.org/10.1016/j.tecto.2015.05.025

Gibling RM, Tantisukrit C, Uttamo W, Thanasuthipitak T, Haraluck M (1985) Oil shale sedimentology and geochemistry in Cenozoic Mae Sot Basin, Thailand. AAPG Bull 69:767–780

Grotzinger JP, Kasting JF (1993) New constraints on Precambrian ocean composition. J Geol 101:235–243

Grotzinger JP, Knoll AH (1999) Stromatolites in Precambrian carbonates: Evolutionary mileposts or environmental dipsticks? Annu Rev Earth Planet Sci 27:313–358

Guo H, Du Y, Kah LC, Huang J, Hu C, Huang H, Yu W (2013) Isotopic composition of organic and inorganic carbon from the Mesoproterozoic Jixian Group, North China: Implications for biological and oceanic evolution. Precambrian Res 224:169–183. https://doi.org/10.1016/j.precamres.2012.09.023

Harazim D, Callow RHT, Mcilroy D (2013) Microbial mats implicated in the generation of intrastratal shrinkage ('synaeresis') cracks. Sedimentology 60:1621–1638. https://doi.org/10.1111/sed.12044

He B, Qiao X (2015) Advances and overview of the study on paleo-earthquake events: A review of seismites. Acta Geol Sin 89:1702–1746

He Z, Song T, Ding X, Zhang Q, Meng X, Ge M (2000) The early syn-sedimentary faulting of the Mesoproterozoic Yanshan Rift and its influence on event sedimentation. J Paleogeogr (chinese Edition) 2:83–91 (**in Chinese with English abstract**)

He B, Jiao C, Cai Z, Liu R, Meert JG, Yun X, Wang T, Chen W, Yu Z, Li J, Peng S, Hao G, Guo X, Qiao X (2021) Soft-sediment deformation structures (SSDS) in the Ediacaran and lower Cambrian succession of the Aksu area, NW Tarim Basin, and their implications. Palaeogeogr Palaeocl Palaeoecol 567:Article 110237.

Hill CM, Corcoran PL (2018) Processes responsible for the development of soft-sediment deformation structures (SSDS) in the Paleoproterozoic Gordon Lake Formation, Huronian Supergroup, Canada. Precambrian Res 310:63–75. https://doi.org/10.1016/j.precamres.2018.02.019

Huang X, Zhu S, He Y (2001) Some Basic Problems in Research on Sequence Stratigraphy of the Meso-Neoproterozoic Strata in Jixian Area. Progr in Precambrian Res 24:201–221

Kaufman A, Xiao S (2003) High CO_2 levels in the Proterozoic atmosphere estimated from analyses of individual microfossils. Nature 425:279–282. https://doi.org/10.1038/nature01902

Li S, Du Y, Zhang Z, Wu J (2008) Earthquake-related soft-sediment deformation structures in Paleogene on the continental shelf of the East China Sea. Front Earth Sci 2:177–186 (**in Chinese with English abstract**)

Li H, Lu S, Su W, Xiang Z, Zhou H, Zhang Y (2013) Recent advances in the study of the Mesoproterozoic geochronology in the North China Craton. J Asian Earth Sci 72:216–227. https://doi.org/10.1016/j.jseaes.2013.02.020

Li H, Su W, Zhou H, Xiang Z, Tian H, Yang L, Huff WD, Ettensohn RF (2014) The first precise age constraints on the Jixian System of the Meso-to Neoproterozoic Standard Section of China: SHRIMP zircon U-Pb dating of bentonites from the Wumishan and Tieling formations in the Jixian Section, North China Craton. Acta Petrol Sin 30:2999–3012 (**in Chinese with English abstract**)

Lu S, Yang C, Li H, Chen Z (2002) North China continent and Columbia supercontinent. Earth Sci Front 9:225–233 (**in Chinese with English abstract**)

Lu K, Bao Z, Ji H, Liu J, Wang G, Ma F, Guo R, Cao Y, Yang F, Fu Y, Li X, Hua Y, Que Y, Li Z, Xu X, Hu X (2019) Characteristics, main controlling factors and favorable area prediction of karstic geothermal reservoirs of the Jixianian Wumishan Formation in Xiong'an New Area. J Paleogeogr (chinese Edition) 21:885–900 (**in Chinese with English abstract**)

Lu K, Bao Z, Sheng M, Bao Y, Dai Q, Cao Y, Liu R, Zhang S, Li J (2021) Influence of internal textures in fracture development in dolostones: A case study in the Mesoproterozoic Wumishan Formation in the Jizhong Depression, Bohai Bay Basin, north China. Mar Petrol Geol 125: Article 104877.

Mei M, Maurice ET (2013) Milankovitch-driven cycles in the Precambrian of China: the Wumishan formation. J Paleogeogr 2:369–389

Mei M, Gao J, Meng Q, Liu Z (2008) Microdigital stromatolites and their response to stromatolite decline at 1250 Ma ± for the Mesoproterozoic Wumishan Formation at Jixian section in Tianjin. J Paleogeogr (chinese Edition) 10:495–509 (**in Chinese with English abstract**)

Obermeier SF (1996) Use of liquefaction-induced features for paleoseismic analysis—an overview of how seismic liquefaction features can be distinguished from other features and how their regional distribution and properties of source sediment can be used to infer the location and strength of Holocene paleo-earthquakes. Eng Geol 44:1–76

Pan J, Qu Y, Ma R, Pan Z, Wang H (2013) Sedimentary and Tectonic Evolution of the Meso-Neoproterozoic Strata in the Northern Margin of the North China Block. Geol J China Univ 19:109–122 (**in Chinese with English abstract**)

Peng P, Zhai M, Zhang H, Zhao T, Ni Z (2004) Geochemistry and geological significance of the 1.8 Ga mafic dyke swarms in the North China Craton: an example from the junction of Shanxi, Hebei and Inner Mongolia. Acta Petrol Sin 20:439–456 (**in Chinese with English abstract**)

Pufahl PK, Pirajno F, Hiatt EE (2013) Riverine mixing and fluvial iron formation: a new type of Precambrian biochemical sediment. Geology 41:1235–1238. https://doi.org/10.1130/G34812.1

Qiao X, Gao L (2007) Mesoproterozoic paleoearthquake and paleogeography in Yan-Liao Aulacogen. J Paleogeogr (chinese Edition) 9:337–352 (**in Chinese with English abstract**)

Qiao X, Li H (2009) Effect of earthquake and ancient earthquake on sediments. J Paleogeogr (chinese Edition) 11:593–610 (**in Chinese with English abstract**)

Qiao X, Guo X, Li H, Guo Z, Su D, Tang Z, Zhang W, Yang G (2012) Soft-sediment deformation in the Late Triassic and the Indosinian tectonic movement in Longmenshan. Acta Geol Sin 86:132–156 (**in Chinese with English abstract**)

Qiao X, Li H, Su D, He B, Tian H, Guo X, Song T, Lv H, Gao L, He J, Yuan X, Zhou W, Zhang M, Sun A, Wang A (2017) Soft Sediment Deformation Structures: Earthquake and Ancient Earthquake Records. Beijing, Geological Publishing House, p. 1–264 (in Chinese).

Rasmussen B, Blake TS, Fletcher IR, Kilburn MR (2009) Evidence for microbial life in synsedimentary cavities from 2.75 Ga terrestrial environments. Geology 37:423–426. https://doi.org/10.1130/G25300A.1

Riding R (2006) Microbial carbonate abundance compared with fluctuations in metazoan diversity over geological time. Sediment Geol 185:229–238

Riding R (2011) Calcified cyanobacteria. In J. Reitner and V. Thiel (eds), Encyclopedia of Geobiology. Encyclopedia of Earth Science Series, Springer, Heidelberg, pp. 211–223.

Rodríguez-Pascua MA, Calvo JP, De Vicente G, Gómez-Gras D (2000) Soft-sediment deformation structures interpreted as seismites in lacustrine sediments of the Prebetic Zone, SE Spain, and their potential use as indicators of earthquake magnitudes during the

Late Miocene. Sediment Geol 135:117–135. https://doi.org/10.1016/S0037-0738(00)00067-1
Rossetti DF (1999) Soft-sediment deformation structures in late Albian to Cenomanian deposits, Sao Luis Basin, northern Brazil: evidence for paleoseismicity. Sedimentology 46:1065–1081
Rossetti DF, Goes AM (2000) Deciphering the sedimentological imprint of paleoseismic events: an example from the Aptian Codo Formation, Northern Brazil. Sediment Geol 135:137–156
Samanta P, Mukhopadhyay S, Mondal A, Sarkar S (2011) Microbial mat structures in profile: The Neoproterozoic Sonia Sandstone, Rajasthan, India. J Asian Earth Sci 40:542–549. https://doi.org/10.1016/j.jseaes.2010.10.008
Shanmugam G (2017) Global case studies of soft-sediment deformation structures (SSDS): Definitions, classifications, advances, origins, and problems. J Paleogeogr 6:251–320. https://doi.org/10.1016/j.jop.2017.06.004
Shen B, Ma H, Ye H, Lang X, Pei H, Zhou C, Yang R (2018) Hydrothermal origin of syndepositional chert bands and nodules in the Mesoproterozoic Wumishan Formation: Implications for the evolution of Mesoproterozoic cratonic basin, North China. Precambrian Res 310:213–228
Song T (1988) A probable earthquake-tsunami sequence in Precambrian carbonate strata of Ming Tombs District, Beijing. Chinese Sci Bull (english Edition) 33:1121–1124
Song T, Gao J (1985) Tidal sedimentary structures from upper precambrian rocks of the Ming Tombs District, Beijing (Peking), China. Precambrian Res 29:93–107. https://doi.org/10.1016/0301-9268(85)90062-2
Su D, Sun A (2011) Soft-sediment deformation and occurrence frequency of paleoearthquake in the Mesoproterozoic Wumishan Formation, Yongding River Valley, Beijing. J Paleogeogr (chinese Edition) 13:593–614 (**in Chinese with English abstract**)
Su D, Sun A (2012) Typical earthquake-induced soft sediment deformation structures in the Mesoproterozoic Wumishan Formation, Yongding River Valley, Beijing, China and interpreted earthquake frequency. J Paleogeogr 1:71–89. https://doi.org/10.3724/SP.J.1261.2012.00007
Tan C, Lu Y, Li X, Song H, Lv D, Ma X, Fan R, Deng S (2021) Carbon, oxygen and strontium isotopes of the Mesoproterozoic Jixian System (1.6-1.4 Ga) in the southern margin of the North China Craton and the geological implications. Int Geol Rev 63:1951–1968
Tang D, Shi X, Pei Y, Jiang G, Zhao G (2011) Redox status of the Mesoproterozoic epeiric sea in North China. J Paleogeogr (chinese Edition) 13:563–580 (**in Chinese with English abstract**)
Tang D, Shi X, Jiang G (2013a) Mesoproterozoic biogenic thrombolites from the North China platform. Int J Earth Sci 102:401–413. https://doi.org/10.1007/s00531-012-0817-9
Tang D, Shi X, Jiang G, Pei Y, Zhang W (2013b) Environment controls on Mesoproterozoic throm- bolite morphogenesis: a case study from the North China Platform. J Paleogeogr 2:275–296
Tang D, Shi X, Jiang G (2014) Sunspot cycles recorded in Mesoproterozoic carbonate biolaminites. Precambrian Res 248:1–16
Tang D, Shi X, Shi Q, Wu J, Song G, Jiang G (2015) Organomineralization in Mesoproterozoic giant ooids. J Asian Earth Sci 107:195–211. https://doi.org/10.1016/j.jseaes.2015.04.034
Tang D, Shi X, Wang X, Jiang G (2016) Extremely low oxygen concentration in mid-Proterozoic shallow seawaters. Precambrian Res 276:145–157. https://doi.org/10.1016/j.precamres.2016.02.005
Tang D, Fu X, Shi X, Zhou L, Zheng W, Li C, Xu D, Zhou X, Xie B, Zhu X, Jiang G (2022) Enhanced weathering triggered the transient oxygenation event at ~1.57 Ga. Geophys Res Lett 49:e2022GL099018. https://doi.org/10.1029/2022GL099018.
Tang D, (2013a) Mesoproterozoic microbialites from North China Platform: microfabrics, organomineralization processes and their paleoenvironmental distribution [Ph.D. thesis]: China University of Geosciences (Beijing). p. 51. 153 p.
Tian H, Zhang Z, Zhang B, Du S, Guo G, Lyu M (2006) Records of paleoseismic events in the res-silk stone bed in Linqu, Shandong. Geol China 33:1137–1143 (**in Chinese with English abstract**)
Trewin NH (1986) Paleoecology and sedimentology of the Achanarras fish bed of the Middle Old Red Sandstone, Scotland. T Roy Soc Edin-Earth Sci 77:21–46
Van Loon AJ (2009) Soft-sediment deformation structures in siliciclastic sediments: an overview. Geologos 15:3–55
Van Loon AJ, Su D (2013) Deformed stromatolites in marbles of the Mesoproterozoic Wumishan Formation as evidence for synsedimentary seismic activity. J Paleogeogr 2:390–401
Xie Q, Zhu X, Hu Q, Chen F, Wang G (1997) Depositional sequence of storm siliceous rock in Wumishan Formation, West Mountain, Beijing, China. Acta Sediment Sin 15:37–40 (**in Chinese with English abstract**)
Yan Y, Liu Z (1998) On the Relationship between biocommunities and paleoenvironments in Changcheng period of the Yan Shan Basin, North China. Acta Micropaleont Sin 15:249–266 (**in Chinese with English abstract**)
Yang H, Chen Z, Papineau D (2022) Cyanobacterial spheroids and other biosignatures from microdigitate stromatolites of Mesoproterozoic Wumishan Formation in Jixian, North China. Precambrian Res 368:Article 106496.
Ying J, Zhou X, Su B, Tang Y (2011) Continental growth and secular evolution: constraints from U-Pb ages and Hf isotope of detrital zircons in Proterozoic Jixian sedimentary section (1.8–0.8 Ga). North China Craton Precambrian Res 189:229–238
Yuan J, Chen X, Tian H (2006) Formation of loop bedding in Jiyang Subbasin, Paleogene. Acta Sediment Sin 24:666–671 (**in Chinese with English abstract**)
Zhai X, Song J, Luo P, Jin T, Wu S, Wang S, Wang G, Li P (2023) Dolomite porosity related to peritidal microbialites textures and facies succession in Mesoproterozoic Wumishan Formation, North China. Precambrian Res 389: Article 107000.
Zhang Y (1985) Stromatolitic microbiota from the middle Proterozoic Wumishan Formation (Jixian Group) of the Ming Tombs, Beijing, China. Precambrian Res 30:277–302. https://doi.org/10.1016/0301-9268(85)90024-5
Zhang C (2004) Hot-tectonic events and evolution of north margin of the North China Craton in Meso-Neoproterozoic. Acta Sci Natur Univ Pek 40:232–240 (**in Chinese with English abstract**)
Zhang W, Li P (1980) Paleomagnetism of the Sinian suberathem in the Jixian, China. Bull Tianjin Inst Geol Miner Resour 1:111–123 (**in Chinese with English abstract**)
Zhang H, Zhang W, Elston PD (1991) Paleomagnetic study on Middle and Late Proterozoic rock in Jixian, North China. Acta Geophys Sin 34:602–615 (**in Chinese with English abstract**)
Zhang C, Wu Z, Gao L, Wang W, Tian Y, Ma C (2007) Earthquake-induced soft-sediment deformation structures in the Mesoproterozoic Wumishan Formation, North China, and their geologic implications. Sci China Ser D Earth Sci 50:350–358 (**in Chinese with English abstract**)
Zhang SH, Li ZX, Evans DAD, Wu HC, Li HY, Dong J (2012) Pre-Rodinia supercontinent Nuna shaping up: a global synthesis with new paleomagnetic results from North China. Earth Planet Sci Lett 353–354:145–155
Zhang Y, Wang C, Wang J (1965) Geological map of Baoding, Heibei, China. National Geological Archives of China. scale 1: 200,000, 1 sheet.
Zhao C, Li R, Zhou J (1997) Sedimentology and Petroleum Geology of the Meso- and Neo-proterozoic in North China. Geological Publishing House, Beijing, pp 143–178
Zhao G, Sun M, Wilde SA, Li S (2003) Assembly, accretion and breakup of the Paleo-Mesoproterozoic Columbia Supercontinent: Records in the North China Craton. Gondwana Res 6:417–434. https://doi.org/10.1016/S1342-937X(05)70996-5

Zhao G, Sun M, Wilde SA, Li S (2004) A Paleo-Mesoproterozoic supercontinent: assembly, growth and breakup. Earth-Sci Rev 67:91–123

Zhao G, Li S, Sun M, Wilde SA (2011) Assembly, accretion, and break-up of the Paleo-Mesoproterozoic Columbia supercontinent: records in the North China Craton revisited. Int Geol Rev 53:1331–1356

Zhong N, Jiang H, Liang L, Xu H, Peng X (2017) Paleoearthquake studies via soft sediment deformation of load, ball-and-pillow structure: A review. Geol Rev 63:719–738 (**in Chinese with English abstract**)